Title

Daytime SO2 chemistry on ubiquitous urban surfaces as a source of organic sulfur compounds in ambient air

Journal

Science Advances, 8(39)

ISSN

2375-2548

Authors

Deng, Huifan
Lakey, Pascale SJ
Wang, Yiqun
et al.

Publication Date

2022-09-30

DOI

10.1126/sciadv.abq6830

Peer reviewed

ATMOSPHERIC SCIENCE

Daytime SO_2 chemistry on ubiquitous urban surfaces as a source of organic sulfur compounds in ambient air

Huifan Deng[1,2,3,4], Pascale S. J. Lakey[5], Yiqun Wang[1,4], Pan Li[1,4], Jinli Xu[1,4], Hongwei Pang[1], Jiangping Liu[1], Xin Xu[6], Xue Li[6,7,8], Xinming Wang[1,2,3], Yuzhong Zhang[9], Manabu Shiraiwa[5], Sasho Gligorovski[1,2,3]*

The reactions of sulfur dioxide (SO_2) with surface-bound compounds on atmospheric aerosols lead to the formation of organic sulfur (OS) compounds, thereby affecting the air quality and climate. Here, we show that the heterogeneous reaction of SO_2 with authentic urban grime under near-ultraviolet sunlight irradiation leads to a large suite of various organic compounds including OS released in the gas phase. Calculations indicate that at the core area of Guangzhou, building surface uptake of SO_2 is 15 times larger than uptake of SO_2 on aerosol surfaces, yielding ~20 ng m^{-3} of OS that represents an important fraction of the observed OS compounds (60 to 200 ng m^{-3}) in ambient aerosols of Chinese megacities. This chemical pathway occurring during daytime can contribute to the observed fraction of OS compounds in aerosols and improve the understanding of haze formation and urban air pollution.

INTRODUCTION

Sulfur dioxide (SO_2) is one of the most important trace gases in the atmosphere emitted by anthropogenic sources such as fossil fuel combustion and occasionally by volcanic eruptions. The mixing ratios of SO_2 in the atmosphere broadly varies, ranging from 20 parts per thousand (ppt) to 1 parts per billion (ppb) in the continental atmosphere, 20 to 50 ppt in the marine boundary layer, several hundreds of parts per billion in urban environments, and parts per million (ppm) levels in volcanic plumes (*1*). Several studies suggested that the heterogeneous and multiphase reactions of SO_2 with organic and inorganic surfaces could contribute substantially to the formation of sulfate ions (SO_4^{2-}) in the atmosphere (*2*–*6*). It is known that sulfate aerosols constitute an important fraction of haze events severely affecting the air quality in densely populated urban environments (*7*–*9*). Sulfate particles exhibit a cooling effect on the global climate by scattering solar radiation and acting as cloud condensation nuclei (*10*–*12*).

Air quality models cannot explain the quick increase in the quantity of sulfate when going from clean air to hazy events and applying only the gas-phase and aqueous-phase chemistry (*8*). A recent air quality model suggested that SO_2 uptake coefficients of 5×10^{-5} can best describe the sulfate formation during severe haze episodes in North of China (*8*).

Urban grime with thicknesses from 10 to 1000 nm deposited on glass windows and concrete walls are abundant in megacities where most of the population lives (*13*–*16*). Urban grime exhibits similar and sometimes even greater surface-to-volume (S/V) ratios than that of atmospheric particulate matter (PM), suggesting that heterogeneous chemistry on urban surfaces can be significant in megacities. Urban grime consists of a mixture of organic compounds, such as polycyclic aromatic hydrocarbons (PAHs) and fatty acids among others, and inorganic salt compounds Na_2SO_4, $NaNO_3$, and NaCl (*16*–*20*).

Uptake coefficients of SO_2 on various organic and inorganic surfaces as a function of relative humidity (RH) (*21*–*23*) have been used as input data to model studies (*8*, *9*, *24*) to integrate heterogeneous reactions of SO_2 with aerosol particles. However, there is still a lack of knowledge about the formation processes of organic sulfur (OS) compounds upon heterogeneous SO_2 oxidation.

Considering the importance of SO_2 heterogeneous conversion to OS compounds, a comprehensive evaluation is required to determine the important factors that govern the heterogeneous kinetics of SO_2 onto atmospherically relevant surfaces. We investigated the heterogeneous uptake of SO_2 by urban grime in the dark and under simulated sunlight irradiation (300 nm < λ < 400 nm) at different RHs and applied a kinetic multilayer model of aerosol surface and bulk chemistry (KM-SUB) (*25*). The formation of the secondary product compounds released in the gas phase was evaluated by real-time measurements of volatile organic compounds (VOCs) by using a secondary electrospray ionization ultrahigh-resolution quadrupole Orbitrap mass spectrometer (SESI-UHR-MS) coupled to a flow tube reactor with urban grime, upon simultaneous exposure to gaseous SO_2 and light irradiation. We observed an unexpectedly high level of VOCs including OS compounds formed during the light-induced heterogeneous processing of SO_2 on the urban grime. Then, we estimated the surface area of urban buildings in the city of Guangzhou on the basis of a building dataset (www.resdc.cn/data.aspx?DATAID=270) that helped to calculate the fluxes of SO_2 by building surfaces. Last, the SO_2 fluxes were used to estimate the contribution of the produced OS fluxes to organosulfur aerosols.

RESULTS

Uptake coefficients of SO_2

The reactive uptake coefficients of SO_2 to the authentic urban grime were calculated from the experimentally measured pseudo–first-order rate constants as follows (*26*–*28*)

[1]State Key Laboratory of Organic Geochemistry and Guangdong Provincial Key Laboratory of Environmental Protection and Resources Utilization, Guangzhou Institute of Geochemistry, Chinese Academy of Sciences, Guangzhou 510 640, China. [2]Guangdong-Hong Kong-Macao Joint Laboratory for Environmental Pollution and Control, Guangzhou Institute of Geochemistry, Chinese Academy of Science, Guangzhou 510640, China. [3]Chinese Academy of Science, Center for Excellence in Deep Earth Science, Guangzhou 510640, China. [4]University of Chinese Academy of Sciences, Beijing, China. [5]Department of Chemistry, University of California, Irvine, Irvine, CA 92687-2025, USA. [6]Institute of Mass Spectrometry and Atmospheric Environment, Jinan University, Guangzhou 510632, China. [7]Guangdong Provincial Engineering Research Center for On-line Source Apportionment System of Air Pollution, Guangzhou 510632, China. [8]Guangdong-Hongkong-Macau Joint Laboratory of Collaborative Innovation for Environmental Quality, Guangzhou 510632, China. [9]Key Laboratory of Coastal Environment and Resources of Zhejiang Province, School of Engineering, Westlake University, Hangzhou 310024, China.
*Corresponding author. Email: gligorovski@gig.ac.cn

$$\gamma = \frac{4\,k_1'}{\bar{v}_{SO_2}}\frac{V}{S} \quad (1)$$

where k_1' (s^{-1}) is the pseudo–first-order rate constant for the heterogeneous reaction between gaseous SO_2 and the urban grime, S (m^2) is the surface of the glass plate, V (m^3) is the volume of the flow tube reactor, and $\bar{v}_{SO_2} = 312$ (m s^{-1}) is the average molecular velocity of SO_2. The uptake coefficients of SO_2 (50 ppb) with urban grime deposited on the glass plates were assessed as a function of RH, in the dark and under ultraviolet-A (UV-A) light irradiation at 296 K (see Materials and Methods and fig. S1).

The uptake coefficients of SO_2 on urban grime in the dark and in the presence of near-UV light increased nonlinearly by more than one order of magnitude from $(1.6 \pm 0.6) \times 10^{-6}$ at 0% RH to $(4.5 \pm 0.5) \times 10^{-5}$ at 90% RH and from $(2.3 \pm 0.01) \times 10^{-6}$ at 0% RH to $(5.0 \pm 0.1) \times 10^{-5}$ at 90% RH, respectively (fig. S2). Similarly, the uptake of SO_2 on oleic acid increased nonlinearly by a factor of 3 from 3.2×10^{-6} at 2% RH to 6.2×10^{-6} at 74% RH under dark conditions, indicating either promoted adsorption of SO_2 or increased SO_2 solubility at higher RH, in both cases enhancing the reaction of SO_2 with oleic acid (*29*).

This behavior is in contrast with the observation by Gen *et al.* (*30*) who reported a slight decrease of the SO_2 (7.7 ppm) uptake coefficients on illuminated nitrate ions (NO_3^-) with RH, from 7.7×10^{-6} at 88% RH to 1.8×10^{-5} at 40% RH. As shown in fig. S2, the uptake coefficients of SO_2 on urban grime in the presence of near-UV light at different RHs are only slightly higher than the uptake in the dark, and they are the same order of magnitude as the photo-induced uptakes of SO_2 (50 ppb) on $PM_{2.5}$ (*6*). However, these values are higher than the uptake of SO_2 on fatty acids under similar conditions (*31*). For example, the uptake of SO_2 (40 ppb) on linoleic acid was reported to be $(5.5 \pm 0.5) \times 10^{-6}$ at 35% RH, as the highest value among the uptake coefficients of SO_2 on different fatty acids (*31*). The uptakes of SO_2 on urban grime are also at least one order of magnitude higher than the SO_2 uptake coefficients on typical mineral particles, such as illite (1.03×10^{-7}), nontronite (0.30×10^{-7}), smectite (1.72×10^{-7}), and Arizona Test Dust (1.37×10^{-7}) (*32*).

Figure S3 shows that the uptake coefficients of SO_2 on urban grime slightly increase with the light intensity. This observation is similar to the report by Zheng *et al.* (*6*) who showed a slight linear increase of SO_2 uptakes with light intensity. Figure S4 indicates that the uptake coefficients of SO_2 on urban grime are independent of the SO_2 mixing ratio at least for atmospherically relevant SO_2 values.

Kinetic modeling of the SO_2 uptakes

The kinetic model reproduced the measured SO_2 uptake coefficients well, providing insights into the processes controlling the loss of SO_2 to urban grime (Fig. 1). Uptake coefficients increase as a function of RH because of increasing diffusion coefficients of SO_2 and fatty acids as the urban grime becomes less viscous. Under dry conditions, the urban grime is likely to be an amorphous solid, and the initial SO_2 reacto-diffusive length is approximately 1 nm, indicating that the reaction only occurs at the surface and near-surface bulk. As the RH increases, the reaction occurs throughout a greater proportion of the 0.19-μm-thick urban grime bulk with the initial SO_2 reacto-diffusive lengths being calculated as 0.020 and 0.018 μm at 90% RH under dark and irradiated conditions, respectively. These findings are similar to our previous work, where NO_2 uptake coefficients on indoor films were found to be dependent on the RH due to changing diffusion in the film (*28*). We were also able to parametrize the SO_2 and fatty acid diffusion coefficients as a function of RH using an exponential function, in a similar fashion to our previous work (*28*), which also reproduced the measurements reasonably well (fig. S5). The obtained bulk reaction rate coefficients were on the order of 10^{-16} to 10^{-18} cm^3 s^{-1}. The rate coefficient of SO_2 with reactive fatty acid was slightly higher for the irradiated condition compared to the dark condition (table S1), reflecting the increase in measured uptake coefficient in the presence of UV light.

The model results are consistent with the experimental measurements that show that the uptake coefficient increases by about a factor of 1.1 to 2.0 in the presence of UV light and over the range of RHs. These enhancements are controlled by the complex interplay of photolysis rates (table S1) and surface composition as moderated by bulk diffusion at different RHs. SO_2 loss from the gas phase was also measured as a function of time and modeled with KM-SUB (fig. S6). Gas-phase SO_2 concentrations at 30% RH were relatively stable over the measurement time scale with the concentrations of the fatty acids also remaining relatively constant (figs. S6, A and B, and S7, A and B). For the 90% RH dark and irradiated conditions, the gas-phase SO_2 concentrations increased over the time period of the measurements (fig. S6, C and D) because of a decreasing loss to the urban grime as the concentration of reactive fatty acid decreased significantly (fig. S7, C and D). At longer times, the gas-phase SO_2 concentration for the 90% RH irradiated condition remained relatively stable and is only controlled by the reaction with fatty acid, which has a relatively stable concentration (fig. S7D). There are some details of the measurements that have not been reproduced by the model such as the faster SO_2 loss observed for the 90% RH dark condition during the first 100 min of reaction (fig. S6C). This may indicate the presence of additional species which are untreated in the model and can react away on this time scale because of a fast reaction with SO_2. Overall, these modeling results suggest that the SO_2 uptake coefficient depends on a variety of factors such as the RH, the concentrations of a variety of reactive species in the urban grime, and the rate of loss and replenishment of these species in urban grime.

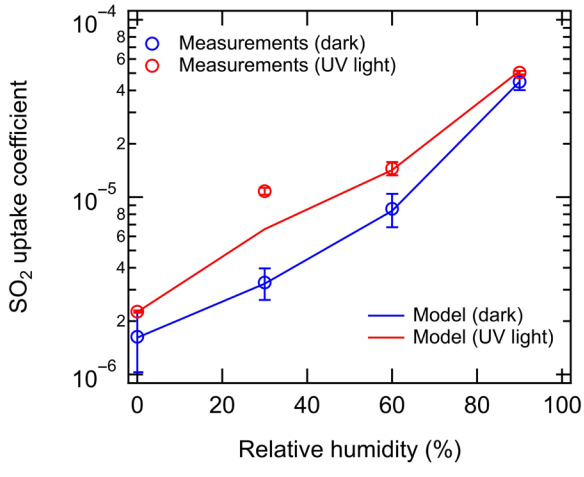

Fig. 1. Measured and modeled SO_2 uptake coefficients on urban grime under dark and irradiated conditions as a function of RH.

General description of gas-phase product compounds

Real-time measurements of the gas-phase compounds formed by the heterogeneous reaction of SO_2 with urban grime at 70% RH, in the dark and under UV-A irradiation, were assessed by a SESI-UHR-MS in both negative (ESI^-) and positive (ESI^+) ionization modes. In addition, blank measurements were performed before and after analysis. Overall, 589 and 58 ions with an intensity threshold above 1×10^5 arbitrary units (a.u.) were distinguished by a Python program (for details, see the Supplementary Materials) in the mass spectra obtained from online measurements in ESI^+ and ESI^- mode, respectively.

A hierarchical cluster analysis was performed to identify the ion groups with different chronological variations (Fig. 2A). Then, in total, 226 ions in the ESI^+ mode and 13 ions in the ESI^- mode were screened out again from the detected compounds above the threshold (1×10^5 a.u.) after deleting the isotope peaks and the significance analysis (two-tailed test). Only the ions with a mass tolerance of ±2 ppm were assigned to the corresponding molecular formulas. The observed peaks in the blank were not considered during the data analysis, regardless of their intensity. Mass spectra in the negative mode often have fewer peaks and are therefore easier to interpret than spectra obtained in the positive mode (*33*). This could be the reason that only 13 ions in total were analyzed in the negative mode. Therefore, the gas-phase products detected in the positive mode will be further discussed.

Figure 2B shows the average mass spectra of the detected product compounds including the relative number abundance of the compounds. To make a comparison among wide range of molecules obtained from the mass spectra, we choose the most abundant $C_{11}H_{21}O_5S_2$ [mass/charge ratio (*m/z*) 297.0824] ion as 100%, and all peak intensities in the measured samples were normalized to it. The attributed elemental formulas are classified into five major compound categories with CH^+-, CHO^+-, $CHOS^+$-, $CHON^+$-, and CHN^+-based formula identification by Xcalibur software (3.0.63, Thermo Fisher Scientific). Of 226 ions the most abundant are CHO^+ with 71.7% followed by 11.5% CH^+, 6.2% $CHOS^+$, 5.3% $CHON^+$, and 1.8% CHN^+, broadly distributed over the whole *m/z* range between 50 and 400 (Fig. 2B). The plausible explanation for the abundance of the CHO compounds could be attributed to the sensitivity of ESI source toward polar oxygenated molecules with lower aromaticity (*34*). Figure 2B (NA, nonavailable) shows that only few substances (3.5%) with a high mass tolerance (> ± 5 ppm) or unknown formulas were observed in this study.

The distribution of the detected ions depicted in the red rectangle of Fig. 2A shows that light-induced heterogeneous processing of SO_2 with 1-month-old urban grime at 70% RH leads to enhanced product formation compared to dark conditions. As an example, Fig. 2C shows the temporal evolution of *m/z* at 101.0596 127.1116, 143.1006, and 153.0909, formed upon SO_2 heterogeneous reaction with urban grime in the dark and under UV-A light irradiation. Paired sample *t* test of *m/z* at 101.0596 127.1116, 143.1006, and 153.0909 (Fig. 2D) shows that there is a significant difference between the concentrations of each ion at zero-air stage and the stage of light-induced SO_2 chemistry of urban grime. The gas-phase product compounds have different chemical properties as illustrated by the Van Krevelen plot depicted in Fig. 3.

The oxygen-to-carbon ratio (O/C) indicates the degree of oxidation, while the hydrogen-to-carbon ratio (H/C) is a good indicator of the degree of unsaturation in organic molecules (*35*). In addition, double bond equivalent (DBE) and aromaticity equivalent (Xc) as important parameters to characterize the chemical composition of the organic components observed by high–mass resolution spectrometry are also shown (Fig. 3). Typically, $2.5 \leq Xc < 2.71$ indicates the presence of monoaromatic compounds, and $Xc \geq 2.71$ suggests the presence of polyaromatic compounds (*36*). Figure 3 shows that many peaks are depicted in the range between $1 < H/C < 2$ and $O/C < 1$, similar to the chemical composition of atmospheric organic aerosols (*37*). Moreover, Fig. 3 shows that compounds with low DBE values (DBE < 6) are abundant, while Xc values range between 0 and 2.5, indicating that most of the observed compounds could be identified as aliphatic compounds with a low degree of aromaticity. One of the reasons for the absence of polyaromatic compounds with high DBE and $Xc \geq 2.71$ is that the ESI ionization method is more sensitive to polar organic compounds instead of nonpolar or less polar compounds such as PAHs and saturated hydrocarbons (*38*). The compounds with high H/C values (>1.5) and low O/C values (<0.5) with DBE = 1, and Xc = 0, could be attributed to aliphatic species (*37*). The left corner at the bottom of Fig. 3 shows the compounds with $H/C \leq 1$, and $O/C \leq 0.5$, which are typically defined as low-oxidation aromatic compounds ($Xc \leq 2.5$) (*39*).

CHO product compounds

The Van Krevelen diagram obtained by plotting the H/C versus O/C ratio for CHO compounds was evaluated more closely in the Fig. 4. Different homolog series of all CHO^+ compounds in the range between $0.6 < H/C < 2$ and $O/C < 0.7$ are displayed in Fig. 4, which have also been detected in coal burning (*40*), cloud water (*41*), and rain water samples (*42*). The continuous homologous CH_2 series indicate their chemical homogeneity. For example, the upper right corner of Fig. 4 shows series of $C_2H_5O_2(CH_2)_n$ and $C_4H_9O(CH_2)_n$ with a low degree of unsaturation (Xc = 0, DBE = 1), which are commonly associated with aliphatic compounds (*42*). Note that CHO-containing compounds emerging from light-induced heterogeneous reaction of SO_2 with urban grime at 70% RH are consistent with the CHO compounds produced during heterogeneous processing of SO_2 with unsaturated fatty acids identified in both field measurements and laboratory experiments (*29*, *31*, *43*). For example, saturated fatty aldehyde with *m/z* 143.1430 [$(C_9H_{18}O)H^+$] (nonanal) and saturated fatty acid *m/z* 145.1222 [$(C_8H_{16}O_2)H^+$] (octanoic acid) were previously identified during the heterogeneous reaction of SO_2 with oleic acid (Fig. 4) (*29*). Unsaturated and saturated fatty acids are the most ubiquitous species [35.8% (5.4 mg m^{-2})], compared to other compounds loaded in the urban grime collected in Guangzhou (fig. S10), the most abundant being nonanoic acid (61.2 μg m^{-2}), among others (table S2). Thus, it is not excluded that compounds such as nonanal are formed upon heterogeneous reaction of SO_2 with nonanoic acid. The heterogeneous reaction of SO_2 with particulate-bound unsaturated fatty acids can lead to the formation of long-chain saturated fatty acids such as *m/z* 227.2006 [$(C_{14}H_{26}O_2)H^+$] (tetradecenoic acid), *m/z* 241.2162 [$(C_{15}H_{28}O_2)H^+$] (pentadecenoic acid), and *m/z* 269.2475 [$(C_{17}H_{32}O_2)H^+$] (heptadecenoic acid) (*43*), which were also identified in this study (table S3), and they belong to the series of $C_3H_5O_2(CH_2)_n$ (Fig. 4).

In addition, fatty acids were proven to act spontaneously as photoactive surfactants under UV light irradiation (*44*). Rossignol *et al.* (*45*) reported a wide variety of mostly oxygenated gas-phase product compounds derived from UV light irradiation of nonanoic acid, including saturated and unsaturated ketones and aldehydes (≤C9). Several fatty aldehydes with the same *m/z* as those reported by

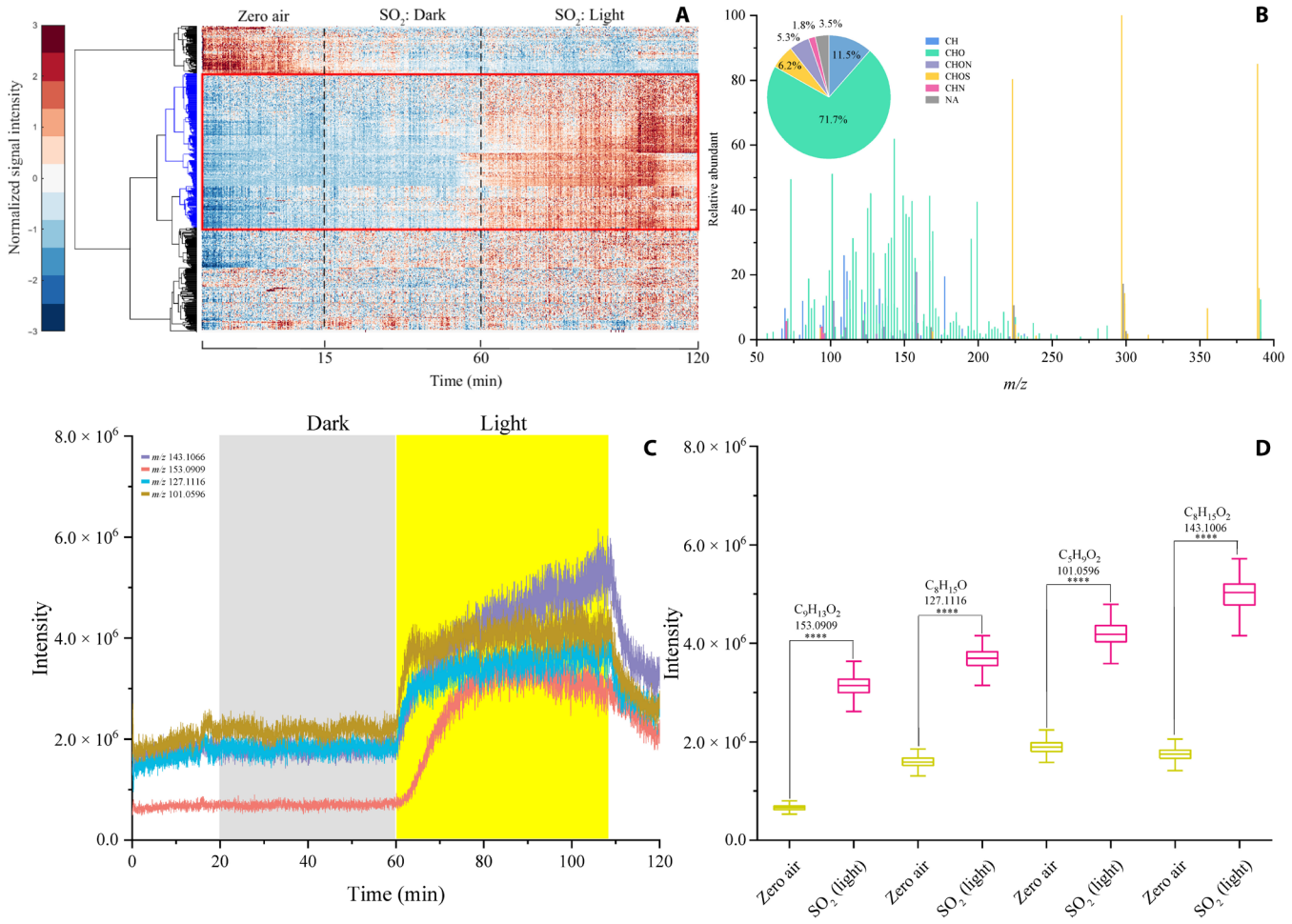

Fig. 2. Mass spectrometric data representing the SO_2 chemistry with urban grime. (**A**) Cluster analysis of 588 ions with signal intensities of ≥1×10^5 a.u. in the positive mode. (**B**) SESI-HR-MS mass spectra in the positive mode. The *x* axis corresponds to the molecular weight of the gas species, and the *y* axis corresponds to the relative abundant. Different formula groups are color-coded. The pie chart shows the proportions of CH^+, CHO^+, $CHON^+$, CHN^+, $CHOS^+$, and unassigned peaks among all observed gas-phase products. (**C**) The time profile of *m/z* at 101.0596, 127.1116, 143.1006, and 153.0909 observed by the SESI-HRMS. (**D**) Box plot of *m/z* at 101.0596, 127.1116, 143.1006, and 153.0909. The paired sample *t* test shows significant difference (****$P < 0.0001$) in signal intensity of each ion at the zero-air stage and stage of SO_2 light-induced processing of urban grime.

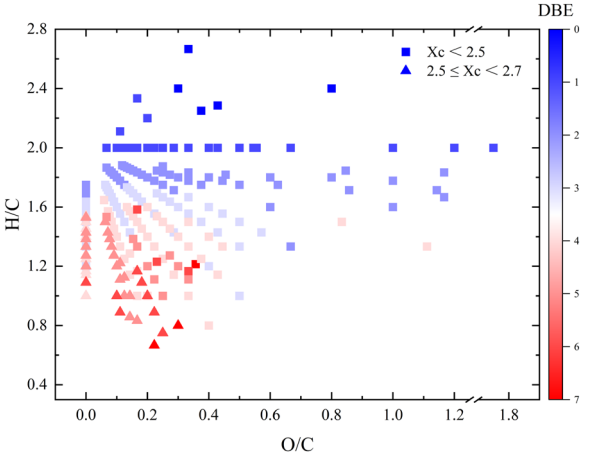

Fig. 3. Van Krevelen plot for the observed organic compounds in ESI^+. The color bar denotes the DBE, and the markers denote the value of Xc divided by different ranges.

Rossignol *et al.* (*45*) were identified in this study—*m/z* 101.0961 [$(C_6H_{12}O)H^+$] (hexanal), *m/z* 115.1117 [$(C_7H_{14}O)H^+$] (heptanal), *m/z* 129.1274 [$(C_8H_{16}O)H^+$] (octanal), and *m/z* 143.1430 [$(C_9H_{18}O)H^+$] (nonanal) (table S3) during light-induced SO_2 heterogeneous processing of urban grime—implying that the presence of nonanoic acid as the most abundant fatty acid in the urban grime is responsible for the production of these aldehydes upon light-induced SO_2 reactions. Several of the chemical formulas (Fig. 4) correspond to compounds (H/C = 2 and O/C < 0.5), which can be also formed upon light irradiation of long-chain saturated fatty acids (*45*).

CHOS product compounds

A total of 14 peaks were assigned to compounds containing C, H, O, and S elements in the ESI^+ mode. More than 88% of CHOS species comprised one S atom and more than four O atoms exhibiting higher molecular weight than the CHO and CHON compounds. Because a sulfate group (–OSO_3H) carries four O atoms and it readily deprotonates in ESI^- mode, these compounds can be assigned to organosulfates as indicated by tandem mass spectrometry (MS/MS) analysis of $\bullet OSO_3^-$ or

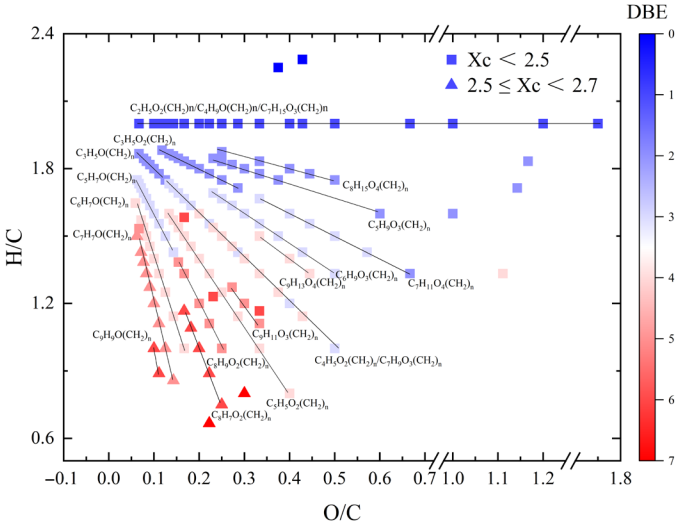

Fig. 4. Van Krevelen plot for homologous series of CHO compounds detected in the ESI$^+$. The "n" refers to the number of CH_2 groups in a given family: (n = 0 to 8)-$C_2H_5O_2^+$, (0 to 10, 12)-$C_3H_5O^+$, (0 to 12, 14)-$C_3H_5O_2^+$, (0, 2 to 6, 11)-$C_4H_9O^+$, (0 to 11)-$C_4H_5O_2^+$, (0 to 11)-$C_5H_7O^+$, (0 to 10)-$C_5H_5O_2^+$, (0, 3 to 8)-$C_5H_9O_3^+$, (0 to 8, 11)-$C_6H_7O^+$, (0 to 7)-$C_6H_9O_3^+$, (0 to 7, 9)-$C_7H_7O^+$, (0 to 6, 8)-$C_7H_9O_3^+$, (0, 5)-$C_7H_{15}O_3^+$, (0 to 3, 5)-$C_7H_{11}O_4^+$, (0 to 4)-$C_8H_7O_2^+$, (0 to 2, 4, 5)-$C_8H_9O_2^+$, (0 to 2, 4, 8)-$C_8H_{15}O_4^+$, (0, 1)-$C_9H_9O^+$, (0 to 2)-$C_9H_{11}O_3^+$, and (0, 1, 3)-$C_9H_{13}O_4^+$. The color bar and marker type denote the DBE values and the Xc range of the compounds.

HSO_4^- product ions (*42*, *46*). However, MS/MS experiments were not performed on the CHOS ions detected, and therefore, other S-containing compounds, such as sulfonates, may also be assigned to this group.

The addition of SO_2 to the double bond of the organic compounds (fatty acids and PAHs) (see Discussion) available on the urban grime could explain the formation of these CHOS compounds. For example, a cycloaddition of SO_2 to the C=C of the PAHs compounds may occur, leading to the formation of cyclic CHOS compounds (*47*–*49*). The observed CHOS could also be organosulfates with a hydroxyl group (OH) and a C=C bond or cycle in the side chain (*46*).

Table S4 shows that most of the CHOS compounds exhibit a low degree of unsaturation and relatively high molecular weights, similar to the composition of OS compounds detected in ambient aerosol samples collected in Guangzhou (*50*, *51*), Wuhan, Nanjing (*52*), and Shanghai (*46*). Previous investigations have suggested that OS compounds with a low degree of unsaturation could be formed via anthropogenic precursors such as long-chain alkanes or aromatic compounds (*46*). It has been reported that long-chain alkanes are major constituents of tailpipe emissions from medium-duty diesel trucks and gasoline-powered motor vehicles in urban areas (*53*). As the urban grime was collected in the downtown of Guangzhou not far from a dense traffic road, it is highly plausible that the origin of the long-chain alkanes and PAHs adsorbed on the urban surface comes from the roadway vehicle emissions. In addition, cooking from the neighboring restaurants (*54*, *55*) can also be an emission source of long-chain alkanes and PAHs (table S2) as possible precursors of the observed organosulfates formed through SO_2 heterogeneous oxidation of the urban grime. The gas chromatography–MS (GC-MS) performed analysis of the sampled urban grime in Guangzhou indicates that the portions of long-chain alkanes and PAHs, which could be responsible for the formation of one fraction of the CHOS compounds, are 7.6 and 1.8%, respectively (fig. S8).

The hydrophilic (sulfate group) and hydrophobic (long alkyl chains) functionalities of the observed CHOS indicate that these compounds have surfactant properties and therefore may substantially affect the aerosol properties (*46*). The following OS compounds detected in this study, *m/z* 95.0160 $[C_2H_6O_2S)H^+]$ (methylsulfonylmethane), *m/z* 169.0523 $[C_5H_{12}O_4S)H^+]$, *m/z* 223.0635 $[(C_8H_{14}O_5S)H^+]$, *m/z* 225.0427 $[(C_7H_{12}O_6S)H^+]$, and *m/z* 239.0948 $[(C_9H_{18}O_5S)H^+]$, were observed in surfactant sulfur-containing aerosols during field measurements in the urban area of Guangzhou (*50*, *51*). The SESI-HR-MS cannot discriminate structural formulas; hence, it is not possible to distinguish whether the CHOS are rather hydroxyl sulfonates or alkyl organosulfates.

The observed OS compounds exhibit a lower degree of unsaturation (low DBE), low degree of oxidation (O/C < 1), and low aromaticity (Xc = 0), indicating that these compounds are most likely aliphatic compounds forming more ordered surfactant films on the aerosols, which would decrease the surface tension and affect the hygroscopicity of the aerosol particles (*46*). It has been suggested that this kind of OS compounds with low degree of unsaturation are representative of urban aerosols in Chinese megacities such as Guangzhou, Shanghai, Wuhan, and Nanjing because of the heavy traffic (*46*, *50*–*52*). It has been suggested that these OS compounds are important constituents of atmospheric aerosol on a global scale and capable of long-range transport (*56*). The CHON, CHN, CH, and unassigned compounds formed upon heterogeneous reaction of SO_2 with urban grime are shown in tables S5 to S7, respectively.

DISCUSSION

The uptakes of SO_2 on urban grime exhibited very similar values and trend in the dark and upon light irradiation, while the product distribution observed in ESI$^+$ mode differs significantly because of the different reaction mechanism between dark and near-UV light conditions (see below). Therefore, a commercial MI-SPI-TOF-MS (membrane inlet-single photon ionization-time of flight-mass spectrometer) device (SPIMS 3000, Guangzhou Hexin Instrument Co. Ltd., China) (see the Supplementary Materials for description) was used to further investigate the impact of the combined effect of RH and presence of light on the formed VOCs upon light-induced heterogeneous reaction of SO_2 with the urban grime. Figure S9 shows the total ion counts (TICs) of the observed gas-phase product compounds by MI-SPI-TOF-MS, upon heterogeneous reaction of SO_2 with urban grime at 0% RH, 30% RH, and 70% RH in the dark and in the presence of light. As shown in fig. S9, the TIC at low RH (0 to 30% RH) slightly increased upon light irradiation, but a sharp increase of TIC was observed at 70% RH. The uptake coefficient of SO_2 also increased with an increase of RH (Fig. 1), indicating that higher RH accelerates SO_2 uptake on urban grime upon light irradiation, leading to enhanced formation of gas-phase product compounds. Considering that the average RH in the Pearl River Delta region (*57*) is about 70% and that haze episodes especially occur at higher RH in the urban atmosphere, the suggested heterogeneous SO_2 chemistry on ubiquitous urban glass surfaces can play an important role during daytime affecting the air quality. In particular, the high RH (70%) would facilitate the reactive uptake of SO_2, leading to the formation of typically polar OS compounds with high water solubility (*43*). The obtained results clearly indicate that synergistic effect of near-UV light irradiation

and high RH (70%) represents key factors promoting the formation of VOCs during the heterogeneous reaction of SO_2 with urban grime.

The formation mechanisms of OS compounds in the atmosphere are not yet fully understood. Some earlier studies suggested that OS compounds might be formed through esterification of OH groups or C=O groups (after gem-diol conversion) with sulfuric acid (*50*, *58*, *59*). However, it has been shown that the esterification reactions between sulfuric acid and simple alcohols are not feasible under typical atmospheric pH conditions (*60*). It was demonstrated that acid-catalyzed reactions of epoxides are kinetically feasible to generate OS compounds (*61*, *62*). It has been also shown that direct addition of SO_2 to C=C bonds of alkenes and fatty acids is another possibility to explain the formation of OS compounds in the atmospheric aerosols (*29*, *31*). The unsaturated fatty acid and PAHs adsorbed on the urban surfaces can react with gaseous SO_2 through a [2 + 2] cycloaddition mechanism leading to the formation of OS compounds (*29*, *31*, *43*). It has to be noted that the forbidden triplet state ($^3B_1$) of SO_2 can be formed upon near-UV light irradiation that lies in the wavelength range between 340 and 400 nm, and it can react with water molecules, leading to the formation of the hydroxyl radical (OH) and hydroxysulfinyl radical (HOSO) (*63*). The OH radical can further oxidize the organic constituents of the urban grime leading to the production of CHO compounds in the air. Under light irradiation, SO_2 can also form π complexes with C=C bonds of fatty acids that can absorb near-UV light, leading to a photoactivation of the fatty acids such as nonanoic acid and generation of saturated and unsaturated aldehydes (*31*). It has been suggested that charge transfer complexes incorporating the excited triplet state of SO_2 ($^3SO_2$*) is the important first step toward product formation during SO_2 reaction with compounds containing C=C bonds (*64*). Following the attack of $^3SO_2$* on the π bond of the fatty acids, oxidation at the carbon radical would be expected to lead to the cyclic sulfite as an intermediate compound (*64*). The diradical organosulfur intermediates can react with O_2 and form reactive oxygen species such as OH, which can initiate radical chain reactions and induce the formation of oxygenated CHO compounds (*29*, *64*). Previous investigations have suggested that the observed compound with *m/z* 189.1122 $[C_9H_{16}O_4)H^+]$ (DBE = 2, Xc = 0) is a common product compound formed upon oxidation of unsaturated lipids (*65*). However, it is difficult to distinguish which pathway is prevailing among all the pathways mentioned above, and it could be responsible for most of the formed OS compounds. Last, it has to be noted that adsorbed ions on the urban grime can also affect the heterogeneous chemistry and alter the reaction mechanism (*27*, *66*, *67*).

Contribution to ambient organosulfur aerosol formation

We evaluate whether heterogeneous reaction of SO_2 with building surfaces may be important for ambient organosulfur aerosol formation. We start from the spatial distribution of building surfaces in a 0.4° × 0.4° (roughly 43 km) domain centering Guangzhou (Fig. 5). We estimate a total building surface area of 0.52 billion m^2. As a comparison, the boundary-layer aerosol surface area is roughly 0.22 billion m^2 for the same study region, if we assume an aerosol concentration of 25 μg m^{-3} (roughly annual mean concentration for Guangzhou), 1-μm aerosol diameter, and 800-m boundary layer height [estimated on the basis of MERRA-2 (modern-era retrospective analysis for research and applications, version 2) reanalysis data].

We then estimate the flux of SO_2 uptake by building or aerosol surfaces (F_i, i = building or aerosol), using the following equation

$$F_i = \frac{1}{4}\gamma_i \omega C_{SO_2} A_i \quad (2)$$

where γ_i is the uptake coefficient (10^{-5} for both building and aerosol surfaces), ω is the mean molecular velocity (312 m s^{-1}), C_{SO2} is the SO_2 concentration (10 μg m^{-3} = 0.16 × 10^{-6} mol m^{-3}), and A_i is the surface area for buildings or aerosols. The above equation does not account for the limitation of gas-phase transport to surfaces, which is, in general, non-negligible for buildings. Nevertheless, $F_{building}$ should still characterize the order of magnitude. We find an average SO_2 uptake flux of 0.06 mol s^{-1} by buildings and 0.03 mol s^{-1} by aerosols over the domain shown in Fig. 5, and the results show that building uptake is up to 15 times faster than aerosol uptake at the city core where high rises locate.

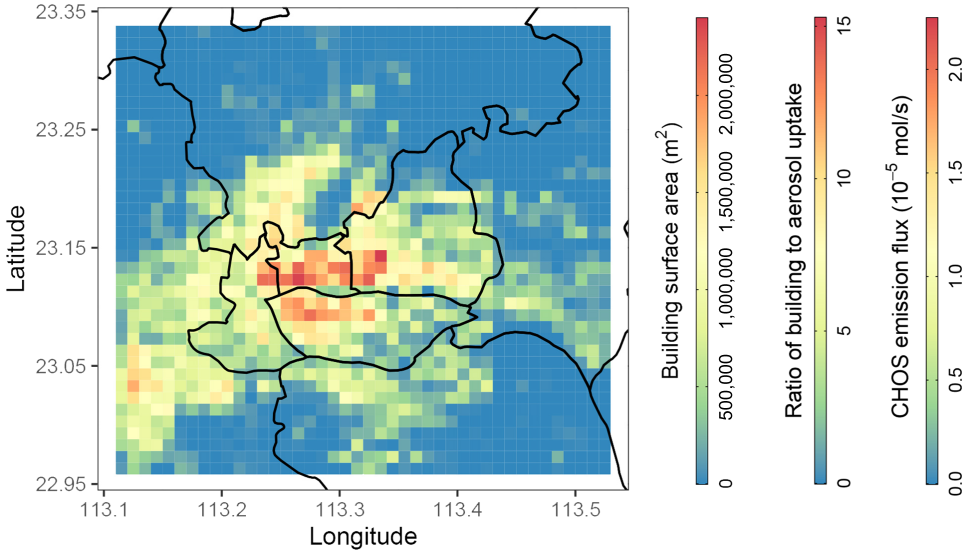

Fig. 5. Distribution of building surface areas, ratio between building surface uptake and aerosol surface uptake, and gaseous CHOS emission fluxes from building surfaces in the city of Guangzhou.

Following the reaction of SO_2 with the urban grime at 70% RH, we have determined (Eq. 7) the concentrations of the produced CHO, CH, CHOS, CHON, and CHN compounds (tables S3 to S5). On the basis of the estimated concentrations, we established the following reaction stoichiometry

$$SO_2 + C{=}C + h\nu \rightarrow 0.35\ CHO + 0.08CHOS + 0.01CHON + 0.05CH + 0.003CHN \quad \text{(R-1)}$$

Assuming that SO_2 reacts with the urban grime by direct addition of SO_2 to a double bond or the separate addition of SO_2 to the cleavage of a double bond (e.g., fatty acids and PAHs) (*31*, *68*), we then estimate a CHOS emission flux of 4.9×10^{-3} mol s^{-1} or an average emission flux density of 2.7×10^{-12} mol m^2 (ground area) s^{-1} from building surfaces in Guangzhou. This emission flux is nontrivial for atmospheric chemistry at the city scale.

We demonstrate this with an order-of-magnitude estimate for the contribution of CHOS fluxes to organosulfur aerosols. We assume that emitted CHOS gases quickly and completely convert into organosulfur aerosols, although the fate of emitted species is not fully addressed in the current study. We treat the domain shown in Fig. 5 as a single well-mixed box with 800-m height, which satisfies the following mass balance equation

$$F_{CHOS}\tau = C_{CHOS}V \quad (3)$$

where τ is the characteristic residence time of the air in the box. τ is roughly 8 hours given a boundary-layer wind speed of 1.8 m s^{-1} (annual mean surface wind speed for Guangzhou) and a lateral length of 43 km. V is the air volume of the box.

This yields an organosulfur concentration (C_{CHOS}) of 1×10^{-10} mol m^{-3} or 20 ng m^{-3} (molecular weight of CHOS molecules is taken roughly as 200 g mol^{-1}) under the average condition in Guangzhou. In comparison, measurements in Guangzhou have shown a CHOS aerosol concentration of 200 ng m^{-3} (*43*). The average concentration of quantified OS compounds in Shanghai was 65.5 to 77.5 ng m^{-3} in 2015 to 2016 and 59.4 to 79.7 ng m^{-3} in 2018 to 2019 (*69*). This result suggests that emissions from building surfaces may be a non-negligible source for OS compounds in megacities through heterogeneous reactions with SO_2 (*70*).

MATERIALS AND METHODS

Urban grime

Sampling of urban grime was carried out in Guangzhou, China between 26 August and 26 September 2020 on the roof of the building situated on the campus of Guangzhou Institute of Geochemistry (113.36° E, 23.13° N), described previously (*26*). Briefly, the building is located about 200 m from a highway with frequent traffic and dense population in metropolitan Guangzhou. The urban film was collected onto rectangular borosilicate glass plates (1.5 cm by 45 cm) by placing them on a custom-built sampler, which shields glass plates from precipitation. Before deployment, borosilicate glass plates were prepared by rinsing eight times with tap water followed by successive immersions into a bath of hydrochloric acid (HCl) of 10%, 1 M sodium hydroxide (NaOH) for 1 hour, and further rinsing eight times in ultrapure water (18 megohms, H_2O-MM-UV-T, Germany), sequentially. Last, they are wrapped in aluminum foil and baked in a 100°C oven to remove any residual moisture. The samples were transported to and from the sampling site and were refrigerated until extraction and further analysis by GC-MS and for assessing the SO_2 heterogeneous reactions in the flow tube reactor.

Flow tube reactor

The flow tube reactor was applied in our previous studies to evaluate the uptake coefficients of NO_2 on urban grime (*26*, *27*, *67*). The uptake coefficients of gaseous SO_2 (50 ppb) with the urban grime were measured in a double-wall flow tube reactor (50-cm length and 2.6-cm inner diameter) coupled to a SO_2 analyzer (Thermo Fisher Scientific, model 43i SO_2 analyzer) under constant ambient temperature (296 K) controlled by a thermostatic bath (Lauda RC6 refrigerated bath with RCS thermostat, temperature accuracy = ± 0.02 K at 263 K). The flow tube reactor is designed to operate at ambient pressure, under gas-phase laminar flow conditions. The glass plate with grime sample was placed in the reactor and exposed to four lamps (Philips TL-D 40 W, 300 to 400 nm, length = 60 cm) that are installed above the reactor and placed in a wooden box. The resulting spectral intensities of the lamps were measured by a calibrated spectroradiometer (Ocean Optics, USA) coupled with a linear-array charge-coupled device detector. All the experiments described here were performed under atmospheric conditions (296 K, 1 atm), and the RH ranged from 0 to 90%. A certified mixture of SO_2 (1 ppm) in nitrogen (N_2) (99.999% MESSER) was connected to a mixing loop fed by synthetic air (99.999% MESSER) to allow dilution. For the first dilution, a constant flow of 25 ml min^{-1} (0 to 100 ml min^{-1} HORIBA METRON Series mass flow controller, ±1% accuracy) of SO_2 flow was introduced into the flow tube through a horizontal movable injector along with synthetic air at a flow rate of 200 ml min^{-1} (0 to 500 ml min^{-1} HORIBA METRON mass flow controller; accuracy, ±1%). Then, a sheath flow of 600 ml min^{-1} (0 to 1000 ml min^{-1} HORIBA METRON mass flow controller; accuracy, ±1%) was provided by a humidifier and incorporated in the reactor to get the second dilution. All gases were taken directly from gas cylinders without further purification before use.

Kinetic modeling

The KM-SUB (*25*) was applied to better understand SO_2 uptake coefficients on urban grime for different RHs and for dark and irradiated conditions. Processes included in the model are SO_2 reversible adsorption to the urban grime surface, surface-bulk exchange, bulk diffusion, and chemical reactions at the surface and in the bulk of the urban grime. The urban grimes may contain various kinds of fatty acids that may have different reactivities toward SO_2. To account for diversity of fatty acids, the model represents them with two surrogate fatty acids with high (fatty acid 1) and low reactivity (fatty acid 2) toward SO_2. Two reactions are included in the model as follows

$$SO_2 + \text{fatty acid 1} \rightarrow \text{product Rate coefficient} = k_1 \quad \text{(R-2)}$$

$$SO_2 + \text{fatty acid 2} \rightarrow \text{product Rate coefficient} = k_2 \quad \text{(R-3)}$$

Rate coefficients for dark and irradiated conditions are assumed to be different in the model. An effective rate coefficient is used for irradiated conditions that may account for potential mechanisms including the formation of the SO_2 triplet state and an SO_2 π complex with alkenes that can be activated by light or species in the urban grime absorbing UV light to take part in photochemical reactions (*31*, *71*). The gas-phase concentration of SO_2 in the flow tube ($[SO_2]_g$) is calculated using the following equation

$$\frac{d[SO_2]_g}{dt} = \frac{\varphi}{V}([SO_2]_{g,0} - [SO_2]_g) - (J_{ads,SO_2} - J_{des,SO_2})\frac{S}{V} \quad (4)$$

where φ is the volumetric flow rate, V is the volume of the flow tube, $[SO_2]_{g,0}$ is the concentration of SO_2 entering the flow tube, J_{ads,SO_2} is the SO_2 adsorption flux, J_{des,SO_2} is the SO_2 desorption flux, and S is the surface area of the urban grime.

Unknown parameters in the model included the rate coefficients (k_1 and k_2) under both dark and irradiated conditions, the thickness of the film, the initial concentrations of the fatty acids in the urban grime, the partitioning coefficient of SO_2 into the urban grime, and the bulk diffusion coefficients of both SO_2 and the fatty acids for different RHs. The Monte Carlo Genetic Algorithm (MCGA) was applied to determine a parameter set that could reproduce the experimental measurements (*72*). During the Monte Carlo runs, parameters are randomly varied between fixed boundaries, and each parameter set is assigned a fitting value based on how well it reproduces the measurements. During the Genetic Algorithm runs, the fitting values of some of the parameter sets are improved using a series of processes known in natural evolution such as survival, recombination, and mutation. The parameter ranges used in the MCGA were based on previous literature whenever possible as described in table S1 (*28*, *73*). Best-fitting parameters used in the model are summarized in table S1. It should be noted that it is not possible to fully constrain all parameters and the range of values that provide a reasonable fit to the experimental data are summarized in figs. S10 to S12.

Sample analysis by GC-MS

Before extract, a piece of sample glass was cut into squares of suitable size a by glass knife and submerged in 30 ml of dichloromethane/methanol (1:1, v/v) and ultrasonically extracted for 5 min, and then the extracts were combined, filtered, and concentrated to about 1 ml at 23°C under N_2 gas. Each of the concentrated extract was split into two aliquots.

The following operation procedure of GC-MS was deployed. In brief, two aliquots were analyzed using an Agilent 7890/5975C gas chromatograph equipped with an HP-5MS capillary column (30 m, 0.25 mm, and 0.25 mm). The temperature program started at 65°C and held for 2 min. Then, the temperature was increased at 5°C min^{-1} to 290°C with a hold at 20 min. Electron impact ionization was used, and a selected-ion monitoring program was developed to quantify all target analytes.

Characterization of gas-phase product compounds

Real-time measurements of the gaseous compounds generated by the heterogeneous reaction of SO_2 with the urban grime were carried out by homemade SESI and detected directly by a high-resolution Q Exactive hybrid Quadrupole Orbitrap mass spectrometer (UHR-MS) (Thermo Fisher Scientific, USA) online coupled to the reactor. Briefly, a modified SESI source from a commercial nano-ESI (Thermo Fisher Scientific, USA) was coupled with a compact stainless steel ionization chamber (*74*, *75*). The chamber was combined with the vacuum interface of the mass spectrometer. The ESI setting parameters in negative and positive modes were as follows: a stable flow rate of 200 ml min^{-1} for a nano-LC system (Thermo Fisher Scientific, USA), 2.5-kV voltage, 90°C for the ionization chamber, and the sampling line heated at 130°C. The mass spectra were obtained in a mass range m/z from 50 to 500 applying a mass resolution of 140,000 at m/z 255 and a scan rate of 1 s. The commercial standard calibration solutions (Thermo Fisher Scientific, USA) were applied to calibrate the Orbitrap mass spectrometer prior to the measurements.

Calculations of the DBE and Xc parameters

To explore the saturation and oxidation degree of the observed compounds, the DBE, aromaticity equivalent (Xc), were calculated. The value of DBE was calculated on the basis of Eq. 5 for the elemental composition CcHhOoNnSs

$$DBE = c - \frac{h}{2} + \frac{n}{2} + 1 \quad (5)$$

where c, h, o, n, and s correspond to the number of carbons, hydrogen, oxygen, nitrogen, and sulfur atoms in the neutral formula, respectively. Molecular formulae with negative DBE and elemental compositions that disobey the nitrogen rule were discarded.

The value of Xc, which is used to identify aromatic and polyaromatic structures in a complex mixture of compounds, was calculated as follows (*36*)

$$Xc = \frac{3[DBE - (m \times o + n \times s)] - 2}{DBE - (m \times o + n \times s)} \quad (6)$$

If DBE ≤ $m \times o + n \times s$ or Xc ≤ 0, then Xc = 0, where m and n correspond to a fraction of O and S atoms in π-bond structures of a compound. When compounds contain functional groups such as aldehydes, ketones, nitroso, cyanate, alcohol, or ethers, m and n are adjusted to 1 or 0 (*36*). We used $m = n = 1$ for the calculation of the Xc in this study.

Estimation of normalized intensity of gaseous product compounds

Assuming equal ionization efficiency of different product compounds, which is commonly used method to estimate O/C ratios of secondary organic aerosols (*51*, *76*, *77*), we calculated the normalized intensity of the formed product compounds during the light-induced SO_2 heterogeneous reaction with authentic urban grime by using 2-butanone as a reference compound (*74*, *78*)

$$C_i = \frac{Int_i}{Int_{BUT}} \times C_{BUT} \quad (7)$$

where C_i is the mixing ratio (pptv or ppbv) of compound i detected during the experiments, Int_{BUT} is the intensity of 2-butanone, Int_i is the intensity of product i, and C_{BUT} is the mixing ratio of 2-butanone, i.e., 2 ppbv. The normalized intensity of the observed compounds can be used as a semiquantitative analysis of the detected product compounds (*79*).

Estimations of building surface areas and OS compound emissions

We first estimated the surface area of urban buildings in the city of Guangzhou on the basis of a building dataset (www.resdc.cn/data.aspx?DATAID=270; accessed April 2022). The dataset contains geocoded building footprints and number of floors for 289,119 buildings around the city center (22.963°N to 23.335°N, 113.115°E to 113.525°E). The surface area of a building is estimated as the sum of its rooftop area and its exterior wall area. The rooftop area is computed as the area of the building footprint, and the exterior wall area is estimated as the perimeter of the building footprint times the

building height (assuming that the average floor height is 3 m). Figure 5 shows the spatial distribution of building surface areas in Guangzhou resolved at 0.01° × 0.01° resolution. High-rise buildings in the core areas result in high surface areas. In total, we estimate a building surface area of 0.52 billion m^2. As a comparison, we estimate that the boundary-layer aerosol surface area is roughly 0.22 billion m^2 for the same study region, if we assume a 25 μg m^{-3} aerosol concentration, 1-μm aerosol diameter, and 800-m boundary layer height (25 μg m^{-3} is close to annual mean aerosol concentration in Guangzhou; annual average boundary layer height based on MERRA-2 reanalysis data).

Given the reaction stoichiometry (R-1), we estimate that the emission fluxes of CHO, CHOS, CHON, CH, and CHN are 2.1×10^{-2}, 4.9×10^{-3}, 6.1×10^{-4}, 3.1×10^{-3}, and 1.8×10^{-4} mol/s, respectively, or the average emission flux densities are 1.2×10^{-11}, 2.7×10^{-12}, 3.4×10^{-13}, 1.7×10^{-12}, and 1.0×10^{-13} mol m^2 (ground area) s^{-1}, respectively. These emission fluxes are nontrivial for atmospheric chemistry at the city scale.

SUPPLEMENTARY MATERIALS

Supplementary material for this article is available at https://science.org/doi/10.1126/sciadv.abq6830

REFERENCE AND NOTES

1. J. M. Anglada, M. T. C. Martins-Costa, J. S. Francisco, M. F. Ruiz-López, Photoinduced oxidation reactions at the air-water interface. *J. Am. Chem. Soc.* **142**, 16140–16155 (2020).
2. T. Y. Liu, A. W. H. Chan, J. P. D. Abbatt, Multiphase oxidation of sulfur dioxide in aerosol particles: Implications for sulfate formation in polluted environments. *Environ. Sci. Technol.* **55**, 4227–4242 (2021).
3. T. Y. Liu, J. P. D. Abbatt, Oxidation of sulfur dioxide by nitrogen dioxide accelerated at the interface of deliquesced aerosol particles. *Nat. Chem.* **13**, 1173–1177 (2021).
4. T. Y. Liu, S. L. Clegg, J. P. D. Abbatt, Fast oxidation of sulfur dioxide by hydrogen peroxide in deliquesced aerosol particles. *Proc. Natl. Acad. Sci. U.S.A.* **117**, 1354–1359 (2020).
5. J. Wang, J. Li, J. Ye, J. Zhao, Y. Wu, J. Hu, D. Liu, D. Nie, F. Shen, X. Huang, D. D. Huang, D. Ji, X. Sun, W. Xu, J. Guo, S. Song, Y. Qin, P. Liu, J. R. Turner, H. C. Lee, S. Hwang, H. Liao, S. T. Martin, Q. Zhang, M. Chen, Y. Sun, X. Ge, D. J. Jacob, Fast sulfate formation from oxidation of SO_2 by NO_2 and HONO observed in Beijing haze. *Nat. Commun.* **11**, 2844 (2020).
6. Y. Zhang, F. Bao, M. Li, H. Xia, D. Huang, C. Chen, J. Zhao, Photoinduced uptake and oxidation of SO_2 on beijing urban $PM_{2.5}$. *Environ. Sci. Technol.* **54**, 14868–14876 (2020).
7. R. J. Huang, Y. L. Zhang, C. Bozzetti, K. F. Ho, J. J. Cao, Y. M. Han, K. R. Daellenbach, J. G. Slowik, S. M. Platt, F. Canonaco, P. Zotter, R. Wolf, S. M. Pieber, E. A. Bruns, M. Crippa, G. Ciarelli, A. Piazzalunga, M. Schwikowski, G. Abbaszade, J. Schnelle-Kreis, R. Zimmermann, Z. S. An, S. Szidat, U. Baltensperger, I. El Haddad, A. S. H. Prévôt, High secondary aerosol contribution to particulate pollution during haze events in China. *Nature* **514**, 218–222 (2014).
8. B. Zheng, Q. Zhang, Y. Zhang, K. B. He, K. Wang, G. J. Zheng, F. K. Duan, Y. L. Ma, T. Kimoto, Heterogeneous chemistry: A mechanism missing in current models to explain secondary inorganic aerosol formation during the January 2013 haze episode in North China. *Atmos. Chem. Phys.* **15**, 2031–2049 (2015).
9. J. Shao, Q. Chen, Y. Wang, X. Lu, P. He, Y. Sun, V. Shah, R. V. Martin, S. Philip, S. Song, Y. Zhao, Z. Xie, L. Zhang, B. Alexander, Heterogeneous sulfate aerosol formation mechanisms during wintertime Chinese haze events: Air quality model assessment using observations of sulfate oxygen isotopes in Beijing. *Atmos. Chem. Phys.* **19**, 6107–6123 (2019).
10. J. Lelieveld, J. Heintzenberg, Sulfate cooling effect on climate through in-cloud oxidation of anthropogenic SO_2. *Science* **258**, 117–120 (1992).
11. J. Heintzenberg, The aerosol-cloud-climate conundrum. *Int. J. Glob. Warm.* **4**, 219–241 (2012).
12. G. H. Wang, R. Y. Zhang, M. E. Gomez, L. X. Yang, M. L. Zamora, M. Hu, Y. Lin, J. F. Peng, S. Guo, J. J. Meng, J. J. Li, C. L. Cheng, T. F. Hu, Y. Q. Ren, Y. S. Wang, J. Gao, J. J. Cao, Z. S. An, W. J. Zhou, G. H. Li, J. Y. Wang, P. F. Tian, W. Marrero-Ortiz, J. Secrest, Z. F. Du, J. Zheng, D. J. Shang, L. M. Zeng, M. Shao, W. G. Wang, Y. Huang, Y. Wang, Y. J. Zhu, Y. X. Li, J. X. Hu, B. Pan, L. Cai, Y. T. Cheng, Y. M. Ji, F. Zhang, D. Rosenfeld, P. S. Liss, R. A. Duce, C. E. Kolb, M. J. Molina, Persistent sulfate formation from London Fog to Chinese haze. *Proc. Natl. Acad. Sci. U.S.A.* **113**, 13630–13635 (2016).
13. A. M. Baergen, D. J. Donaldson, Photochemical renoxification of nitric acid on real urban grime. *Environ. Sci. Technol.* **47**, 815–820 (2013).
14. A. M. Baergen, D. J. Donaldson, Formation of reactive nitrogen oxides from urban grime photochemistry. *Atmos. Chem. Phys.* **16**, 6355–6363 (2016).
15. A. M. Baergen, S. A. Styler, D. van Pinxteren, K. Muller, H. Herrmann, D. J. Donaldson, Chemistry of urban grime: Inorganic ion composition of grime vs particles in Leipzig, Germany. *Environ. Sci. Technol.* **49**, 12688–12696 (2015).
16. S. A. Styler, A. M. Baergen, D. J. Donaldson, H. Herrmann, Organic composition, chemistry, and photochemistry of urban film in Leipzig, Germany. *ACS Earth and Space Chem.* **2**, 935–945 (2018).
17. M. L. Diamond, S. E. Gingrich, K. Fertuck, B. E. McCarry, G. A. Stern, B. Billeck, B. Grift, D. Brooker, T. D. Yager, Evidence for organic film on an impervious urban surface: Characterization and potential teratogenic effects. *Environ. Sci. Technol.* **34**, 2900–2908 (2000).
18. S. E. Gingrich, M. L. Diamond, Atmospherically derived organic surface films along an urban-rural gradient. *Environ. Sci. Technol.* **35**, 4031–4037 (2001).
19. B. Lam, M. L. Diamond, A. J. Simpson, P. A. Makar, J. Truong, N. A. Hernandez-Martinez, Chemical composition of surface films on glass windows and implications for atmospheric chemistry. *Atmos. Environ.* **39**, 6578–6586 (2005).
20. S. H. Pan, J. Li, T. Lin, G. Zhang, X. D. Li, H. Yin, Polycyclic aromatic hydrocarbons on indoor/outdoor glass window surfaces in Guangzhou and Hong Kong, south China. *Environ. Pollut.* **169**, 190–195 (2012).
21. J. H. Ye, J. P. D. Abbatt, A. W. H. Chan, Novel pathway of SO_2 oxidation in the atmosphere: Reactions with monoterpene ozonolysis intermediates and secondary organic aerosol. *Atmos. Chem. Phys.* **18**, 5549–5565 (2018).
22. D. Urupina, J. Lasne, M. N. Romanias, V. Thiery, P. Dagsson-Waldhauserova, F. Thevenet, Uptake and surface chemistry of SO_2 on natural volcanic dusts. *Atmos. Environ.* **217**, 116942 (2019).
23. W. Wang, M. Liu, T. Wang, Y. Song, L. Zhou, J. Cao, J. Hu, G. Tang, Z. Chen, Z. Li, Z. Xu, C. Peng, C. Lian, Y. Chen, Y. Pan, Y. Zhang, Y. Sun, W. Li, T. Zhu, H. Tian, M. Ge, Sulfate formation is dominated by manganese-catalyzed oxidation of SO_2 on aerosol surfaces during haze events. *Nat. Commun.* **12**, 1993 (2021).
24. Y. X. Wang, Q. Q. Zhang, J. K. Jiang, W. Zhou, B. Y. Wang, K. B. He, F. K. Duan, Q. Zhang, S. Philip, Y. Y. Xie, Enhanced sulfate formation during China's severe winter haze episode in January 2013 missing from current models. *J. Geophys. Res. Atmos.* **119**, 10,425–10,440 (2014).
25. M. Shiraiwa, C. Pfrang, U. Poschl, Kinetic multi-layer model of aerosol surface and bulk chemistry (KM-SUB): The influence of interfacial transport and bulk diffusion on the oxidation of oleic acid by ozone. *Atmos. Chem. Phys.* **10**, 3673–3691 (2010).
26. J. Liu, S. Li, M. Mekic, H. Jiang, W. Zhou, G. Loisel, W. Song, X. Wang, S. Gligorovski, Photoenhanced uptake of NO_2 and HONO formation on real urban grime. *Environ. Sci. Technol. Lett.* **6**, 413–417 (2019).
27. J. Liu, H. Deng, S. Li, H. Jiang, M. Mekic, W. Zhou, Y. Wang, G. Loisel, X. Wang, S. Gligorovski, Light-enhanced heterogeneous conversion of NO_2 to HONO on solid films consisting of fluorene and fluorene/Na_2SO_4: An impact on urban and indoor atmosphere. *Environ. Sci. Technol.* **54**, 11079–11086 (2020).
28. J. Liu, H. Deng, P. S. J. Lakey, H. Jiang, M. Mekic, X. Wang, M. Shiraiwa, S. Gligorovski, Unexpectedly high indoor HONO concentrations associated with photochemical NO_2 transformation on glass windows. *Environ. Sci. Technol.* **54**, 15680–15688 (2020).
29. J. Shang, M. Passananti, Y. Dupart, R. Ciuraru, L. Tinel, S. Rossignol, S. Perrier, T. Zhu, C. George, SO_2 uptake on oleic acid: A new formation pathway of organosulfur compounds in the atmosphere. *Environ. Sci. Technol. Lett.* **3**, 67–72 (2016).
30. M. Gen, R. Zhang, D. D. Huang, Y. Li, C. K. Chan, Heterogeneous oxidation of SO_2 in sulfate production during nitrate photolysis at 300 nm: Effect of pH, relative humidity, irradiation intensity, and the presence of organic compounds. *Environ. Sci. Technol.* **53**, 8757–8766 (2019).
31. M. Passananti, L. Kong, J. Shang, Y. Dupart, S. Perrier, J. Chen, D. J. Donaldson, C. George, Organosulfate formation through the heterogeneous reaction of sulfur dioxide with unsaturated fatty acids and long-chain alkenes. *Angew. Chem. Int. Ed. Engl.* **55**, 10336–10339 (2016).
32. K. Wang, Y. Zhang, R. J. Huang, M. Wang, H. Ni, C. J. Kampf, Y. Cheng, M. Bilde, M. Glasius, T. Hoffmann, Molecular characterization and source identification of atmospheric particulate organosulfates using ultrahigh resolution mass spectrometry. *Environ. Sci. Technol.* **53**, 6192–6202 (2019).
33. S. A. Nizkorodov, J. Laskin, A. Laskin, Molecular chemistry of organic aerosols through the application of high resolution mass spectrometry. *Phys. Chem. Chem. Phys.* **13**, 3612–3629 (2011).
34. C. P. West, A. P. S. Hettiyadura, A. Darmody, G. Mahamuni, J. Davis, I. Novosselov, A. Laskin, Molecular composition and the optical properties of brown carbon generated by the ethane flame. *ACS Earth Space Chem.* **4**, 1090–1103 (2020).
35. D. E. Romonosky, A. Laskin, J. Laskin, S. A. Nizkorodov, High-resolution mass spectrometry and molecular characterization of aqueous photochemistry products of common types of secondary organic aerosols. *J. Phys. Chem. A* **119**, 2594–2606 (2015).

36. M. M. Yassine, M. Harir, E. Dabek-Zlotorzynska, P. Schmitt-Kopplin, Structural characterization of organic aerosol using Fourier transform ion cyclotron resonance mass spectrometry: Aromaticity equivalent approach. *Rapid Commun. Mass Spectrom.* **28**, 2445–2454 (2014).
37. C. Zuth, A. L. Vogel, S. Ockenfeld, R. Huesmann, T. Hoffmann, Ultrahigh-resolution mass spectrometry in real time: Atmospheric pressure chemical ionization orbitrap mass spectrometry of atmospheric organic aerosol. *Anal. Chem.* **90**, 8816–8823 (2018).
38. P. Lin, L. T. Fleming, S. A. Nizkorodov, J. Laskin, A. Laskin, Comprehensive molecular characterization of atmospheric brown carbon by high resolution mass spectrometry with electrospray and atmospheric pressure photoionization. *Anal. Chem.* **90**, 12493–12502 (2018).
39. W. Wang, Y. Zhang, B. Jiang, Y. Chen, Y. Song, Y. Tang, C. Dong, Z. Cai, Molecular characterization of organic aerosols in Taiyuan, China: Seasonal variation and source identification. *Sci. Total Environ.* **800**, 149419 (2021).
40. J. Song, M. Li, X. Fan, C. Zou, M. Zhu, B. Jiang, Z. Yu, W. Jia, Y. Liao, P. Peng, Molecular characterization of water- and methanol-soluble organic compounds emitted from residential coal combustion using ultrahigh-resolution electrospray ionization fourier transform ion cyclotron resonance mass spectrometry. *Environ. Sci. Technol.* **53**, 13607–13617 (2019).
41. Y. Zhao, A. G. Hallar, L. R. Mazzoleni, Atmospheric organic matter in clouds: Exact masses and molecular formula identification using ultrahigh-resolution FT-ICR mass spectrometry. *Atmos. Chem. Phys.* **13**, 12343–12362 (2013).
42. P. Lin, A. G. Rincon, M. Kalberer, J. Z. Yu, Elemental composition of HULIS in the pearl river delta Region, China: Results inferred from positive and negative electrospray high resolution mass spectrometric data. *Environ. Sci. Technol.* **46**, 7454–7462 (2012).
43. M. Zhu, B. Jiang, S. Li, Q. Yu, X. Yu, Y. Zhang, X. Bi, J. Yu, C. George, Z. Yu, X. Wang, Organosulfur compounds formed from heterogeneous reaction between SO_2 and particulate-bound unsaturated fatty acids in ambient air. *Environ. Sci. Technol. Lett.* **6**, 318–322 (2019).
44. J. Lin, Q. Dai, H. Zhao, H. Cao, T. Wang, G. Wang, C. Chen, Photoinduced release of volatile organic compounds from fatty alcohols at the air-water interface: The role of singlet oxygen photosensitized by a carbonyl group. *Environ. Sci. Technol.* **55**, 8683–8690 (2021).
45. S. Rossignol, L. Tinel, A. Bianco, M. Passananti, M. Brigante, D. J. Donaldson, C. George, Atmospheric photochemistry at a fatty acid-coated air-water interface. *Sci. Adv.* **353**, 699–702 (2016).
46. S. Tao, X. Lu, N. Levac, A. P. Bateman, T. B. Nguyen, D. L. Bones, S. A. Nizkorodov, J. Laskin, A. Laskin, X. Yang, Molecular characterization of organosulfates in organic aerosols from Shanghai and Los Angeles urban areas by nanospray-desorption electrospray ionization high-resolution mass spectrometry. *Environ. Sci. Technol.* **48**, 10993–11001 (2014).
47. L. J. Andrews, R. M. Keefer, The interaction of sulfur dioxide with aromatic substances. *J. Am. Chem. Soc.* **73**, 4169–4172 (1951).
48. M. Christl, E. Brunn, F. Lanzendoerfer, Reactions of benzvalene with tetracyanoethylene, 2,3-dichloro-5,6-dicyano-p-benzoquinone, chlorosulfonyl isocyanate, and sulfur dioxide. Evidence for concerted 1,4-cycloadditions to a vinylcyclopropane system. *J. Am. Chem. Soc.* **106**, 373–382 (1984).
49. P. Vogel, M. Turks, L. Bouchez, D. Markovic, A. Varela-Alvarez, J. A. Sordo, New organic chemistry of sulfur dioxide. *Acc. Chem. Res.* **40**, 931–942 (2007).
50. B. Y. Kuang, P. Lin, M. Hu, J. Z. Yu, Aerosol size distribution characteristics of organosulfates in the Pearl River Delta Region, China. *Atmos. Environ.* **130**, 23–35 (2016).
51. P. Lin, J. Z. Yu, G. Engling, M. Kalberer, Organosulfates in humic-like substance fraction isolated from aerosols at seven locations in East Asia: A study by ultra-high-resolution mass spectrometry. *Environ. Sci. Technol.* **46**, 13118–13127 (2012).
52. X. K. Wang, S. Rossignol, Y. Ma, L. Yao, M. Y. Wang, J. M. Chen, C. George, L. Wang, Molecular characterization of atmospheric particulate organosulfates in three megacities at the middle and lower reaches of the Yangtze River. *Atmos. Chem. Phys.* **16**, 2285–2298 (2016).
53. M. J. K. James, J. Schauer, G. R. Cass, B. R. T. Simoneit, Measurement of emissions from air pollution sources. 5. C_1–C_{32} organic compounds from gasoline-powered motor vehicles. *Environ. Sci. Technol.* **36**, 1169–1180 (2002).
54. L. Y. He, Y. Lin, X. F. Huang, S. Guo, L. Xue, Q. Su, M. Hu, S. J. Luan, Y. H. Zhang, Characterization of high-resolution aerosol mass spectra of primary organic aerosol emissions from Chinese cooking and biomass burning. *Atmos. Chem. Phys.* **10**, 11535–11543 (2010).
55. R. Siddique, A. F. Zahoor, H. Ahmad, F. M. Zahid, E. Karrar, Impact of different cooking methods on polycyclic aromatic hydrocarbons in rabbit meat. *Food Sci. Nutr.* **9**, 3219–3227 (2021).
56. T. Reemtsma, A. These, P. Venkatachari, X. Xia, P. K. Hopke, A. Springer, M. Linscheid, Identification of fulvic acids and sulfated and nitrated analogues in atmospheric aerosol by electrospray ionization fourier transform ion cyclotron resonance mass spectrometry. *Anal. Chem.* **78**, 8299–8304 (2006).
57. X. X. Fu, X. M. Wang, Q. H. Hu, G. H. Li, X. Ding, Y. L. Zhang, Q. F. He, T. Y. Liu, Z. Zhang, Q. Q. Yu, R. Q. Shen, X. H. Bi, Changes in visibility with $PM_{2.5}$ composition and relative humidity at a background site in the Pearl River Delta region. *J. Environ. Sci. (China)* **40**, 10–19 (2016).
58. J. Liggio, S. M. Li, Organosulfate formation during the uptake of pinonaldehyde on acidic sulfate aerosols. *Geophys. Res. Lett.* **33**, L13808 (2006).
59. J. D. Surratt, J. H. Kroll, T. E. Kleindienst, E. O. Edney, M. Claeys, A. Sorooshian, N. L. Ng, J. H. Offenberg, M. Lewandowski, M. Jaoui, R. C. Flagan, J. H. Seinfeld, Evidence for organosulfates in secondary organic aerosol. *Environ. Sci. Technol.* **41**, 517–527 (2007).
60. E. C. Minerath, M. T. Casale, M. J. Elrod, Kinetics feasibility study of alcohol sulfate esterification reactions in tropospheric aerosols. *Environ. Sci. Technol.* **42**, 4410–4415 (2008).
61. E. C. Minerath, M. J. Elrod, Assessing the potential for diol and hydroxy sulfate ester formation from the reaction of epoxides in tropospheric aerosols. *Environ. Sci. Technol.* **43**, 1386–1392 (2009).
62. E. C. Minerath, M. P. Schultz, M. J. Elrod, Kinetics of the reactions of isoprene-derived epoxides in model tropospheric aerosol solutions. *Environ. Sci. Technol.* **43**, 8133–8139 (2009).
63. J. A. Kroll, B. N. Frandsen, R. J. Rapf, H. G. Kjaergaard, V. Vaida, Reactivity of electronically excited SO_2 with alkanes. *J. Phys. Chem. A* **122**, 7782–7789 (2018).
64. P. W. Jones, A. H. Adelman, A novel preparation of cyclic sulfites through photosulfoxidation of alkenes. *Tetrahedron* **30**, 2053–2055 (1974).
65. E. N. Frankel, Volatile lipid oxidation-products. *J. Am. Oil Chem. Soc.* **59**, 1–33 (1982).
66. M. I. Guzman, R. R. Athalye, J. M. Rodriguez, Concentration effects and ion properties controlling the fractionation of halides during aerosol formation. *J. Phys. Chem. A* **116**, 5428–5435 (2012).
67. H. Deng, J. Liu, Y. Wang, W. Song, X. Wang, X. Li, D. Vione, S. Gligorovski, Effect of inorganic salts on n-containing organic compounds formed by heterogeneous reaction of NO_2 with oleic acid. *Environ. Sci. Technol.* **55**, 7831–7840 (2021).
68. S. Wagner, T. Riedel, J. Niggemann, A. V. Vähätalo, T. Dittmar, R. Jaffe, Linking the molecular signature of heteroatomic dissolved organic matter to watershed characteristics in world rivers. *Environ. Sci. Technol.* **49**, 13798–13806 (2015).
69. Y. Wang, Y. Zhao, Y. Wang, J.-Z. Yu, J. Shao, P. Liu, W. Zhu, Z. Cheng, Z. Li, N. Yan, H. Xiao, Organosulfates in atmospheric aerosols in Shanghai, China: Seasonal and interannual variability, origin, and formation mechanisms. *Atmos. Chem. Phys.* **21**, 2959–2980 (2021).
70. E. A. Pillar-Little, M. I. Guzman, An overview of dynamic heterogeneous oxidations in the troposphere. *Environments* **5**, 104 (2018).
71. C. R. Kroptavich, S. Zhou, S. F. Kowal, T. F. Kahan, Physical and chemical characterization of urban grime sampled from two cities. *ACS Earth Space Chem.* **4**, 1813–1822 (2020).
72. T. Berkemeier, M. Ammann, U. K. Krieger, T. Peter, P. Spichtinger, U. Pöschl, M. Shiraiwa, A. J. Huisman, Technical note: Monte Carlo genetic algorithm (MCGA) for model analysis of multiphase chemical kinetics to determine transport and reaction rate coefficients using multiple experimental data sets. *Atmos. Chem. Phys.* **17**, 8021–8029 (2017).
73. M. Shiraiwa, M. Ammann, T. Koop, U. Pöschl, Gas uptake and chemical aging of semisolid organic aerosol particles. *Proc. Natl. Acad. Sci. U.S.A.* **108**, 11003–11008 (2011).
74. J. Zeng, Z. Yu, M. Mekic, J. Liu, S. Li, G. Loisel, W. Gao, A. Gandolfo, Z. Zhou, X. Wang, H. Herrmann, S. Gligorovski, X. Li, Evolution of indoor cooking emissions captured by using secondary electrospray ionization high-resolution mass spectrometry. *Environ. Sci. Technol. Lett.* **7**, 76–81 (2020).
75. M. Mekic, J. F. Zeng, B. Jiang, X. Li, Y. G. Lazarou, M. Brigante, H. Herrmann, S. Gligorovski, Formation of toxic unsaturated multifunctional and organosulfur compounds from the photosensitized processing of fluorene and DMSO at the air-water interface. *J. Geophys. Res. Atmos.* **125**, e2019JD031839 (2020).
76. A. P. Bateman, J. Laskin, A. Laskin, S. A. Nizkorodov, Applications of high-resolution electrospray ionization mass spectrometry to measurements of average oxygen to carbon ratios in secondary organic aerosols. *Environ. Sci. Technol.* **46**, 8315–8324 (2012).
77. D. O. De Haan, A. Pajunoja, L. N. Hawkins, H. G. Welsh, N. G. Jimenez, A. De Loera, M. Zauscher, A. D. Andretta, B. W. Joyce, A. C. De Haan, M. Riva, T. Q. Cui, J. D. Surratt, M. Cazaunau, P. Formenti, A. Gratien, E. Pangui, J. F. Doussin, Methylamine's effects on methylglyoxal-containing aerosol: Chemical, physical, and optical changes. *ACS Earth and Space Chem.* **3**, 1706–1716 (2019).
78. J. Zeng, M. Mekic, X. Xu, G. Loisel, Z. Zhou, S. Gligorovski, X. Li, A novel insight into the ozone-skin lipid oxidation products observed by secondary electrospray ionization high-resolution mass spectrometry. *Environ. Sci. Technol.* **54**, 13478–13487 (2020).
79. B. R. G. Mabato, Y. Lyu, Y. Ji, Y. J. Li, D. D. Huang, X. Li, T. Nah, C. H. Lam, C. K. Chan, Aqueous secondary organic aerosol formation from the direct photosensitized oxidation of vanillin in the absence and presence of ammonium nitrate. *Atmos. Chem. Phys.* **22**, 273–293 (2022).
80. J. P. Liu, S. Li, J. F. Zeng, M. Mekic, Z. J. Yu, W. T. Zhou, G. Loisel, A. Gandolfo, W. Song, X. M. Wang, Z. Zhou, H. Herrmann, X. Li, S. Gligorovski, Assessing indoor gas phase oxidation capacity through real-time measurements of HONO and NO_x in Guangzhou, China. *Environ Sci Process Impacts* **21**, 1393–1402 (2019).

81. Z. J. Yu, C. Liu, H. Z. Niu, M. M. Wu, W. Gao, Z. Zhou, Z. X. Huang, X. Li, Real time analysis of trace volatile organic compounds in ambient air: A comparison between membrane inlet single photon ionization mass spectrometry and proton transfer reaction mass spectrometry. *Anal. Methods* **12**, 4343–4350 (2020).
82. H. Jiang, L. Carena, Y. He, Y. Wang, W. Zhou, L. Yang, T. Luan, X. Li, M. Brigante, D. Vione, S. Gligorovski, Photosensitized degradation of DMSO initiated by PAHs at the air-water interface, as an alternative source of organic sulfur compounds to the atmosphere. *J. Geophys. Res. Atmos.* **126**, e2021JD035346 (2021).
83. P. Li, H. Pang, Y. Wang, H. Deng, J. Liu, G. Loisel, B. Jin, X. Li, D. Vione, S. Gligorovski, Inorganic ions enhance the number of product compounds through heterogeneous processing of gaseous NO_2 on an aqueous layer of acetosyringone. *Environ. Sci. Technol.* **56**, 5398–5408 (2022).
84. H. Jiang, Y. He, Y. Wang, S. Li, B. Jiang, L. Carena, X. Li, L. Yang, T. Luan, D. Vione, S. Gligorovski, Formation of organic sulfur compounds through SO_2-initiated photochemistry of PAHs and dimethylsulfoxide at the air-water interface. *Atmos. Chem. Phys.* **22**, 4237–4252 (2022).
85. K. Wang, Y. Zhang, R.-J. Huang, J. Cao, T. Hoffmann, UHPLC-orbitrap mass spectrometric characterization of organic aerosol from a central European city (Mainz, Germany) and a Chinese megacity (Beijing). *Atmos. Environ.* **189**, 22–29 (2018).
86. M. Teich, D. van Pinxteren, M. Wang, S. Kecorius, Z. Wang, T. Müller, G. Močnik, H. Herrmann, Contributions of nitrated aromatic compounds to the light absorption of water-soluble and particulate brown carbon in different atmospheric environments in Germany and China. *Atmos. Chem. Phys.* **17**, 1653–1672 (2017).

Acknowledgments
Funding: This work was financially supported by the National Natural Science Foundation of China (no. 42177087 and 41977187), Chinese Academy of Science, International Cooperation Grant (no. 132744KYSB20190007), State Key Laboratory of Organic Geochemistry, Guangzhou Institute of Geochemistry (SKLOG2020-5 and KTZ_17101), and the Guangdong Foundation for Program of Science and Technology Research (no. 2017B030314057). M.S. acknowledges funding from Alfred P. Sloan Foundation (MOCCIE 3, G-2020-13912). **Author contributions:** Conceptualization: S.G. Methodology: H.D., P.S.J.L., M.S., Y.Z., and S.G. Investigation: H.D., P.S.J.L., Y.W., P.L., J.X., H.P., J.L., and X.X. Supervision: S.G., X.L., X.W., Y.Z., and M.S. Writing (original draft): H.D. and S.G. Writing (review and editing): H.D., P.S.J.L., M.S., Y.Z., and S.G. **Competing interests:** The authors declare that they have no competing interests. **Data and materials availability:** All data needed to evaluate the conclusions in the paper are present in the paper and/or the Supplementary Materials.

Submitted 25 April 2022
Accepted 10 August 2022
Published 28 September 2022
10.1126/sciadv.abq6830